Article

Structures and Properties of MgTiH$_n$ Clusters ($n \leq 20$)

Camryn Newland [1], D. Balamurugan [2] and Jonathan T. Lyon [1,*]

1 Department of Chemistry, Murray State University, Murray, KY 42071, USA
2 Office of Advanced Research Computing, Rutgers University, Piscataway, NJ 08854, USA
* Correspondence: jlyon6@murraystate.edu; Tel.: +1-270-809-5378

Abstract: Magnesium hydride solids doped with transition metals have received attention recently as prospective hydrogen storage materials for a green energy source and a hydrogen economy. In this study, MgTiH$_n$ (n = 1–20) clusters were investigated for the first time by employing the B3PW91 hybrid density functional theory computational chemistry technique with all electron basis sets to determine precise cluster structures and the maximum hydrogen capacity for this model system. We find that hydrogen atoms bind to the metal cluster core until a MgTiH$_{14}$ saturation limit is reached, with hydrogen dissociation from this system occurring for MgTiH$_{15}$ and larger cluster sizes. This MgTiH$_{14}$ cluster contains a large 16.4% hydrogen by mass. This saturation size limit and hydrogen mass percent is larger than the analogous MgScH$_n$ system previously reported. The clusters relative stabilities and electronic properties are discussed along with a possible novel hydrogen dissociation pathway. MgTiH$_{10}$ and MgTiH$_{13}$ clusters are predicted to be especially stable species in this size range.

Keywords: clusters; density functional theory; global optimization; doped magnesium hydride; solid-state material; hydrogen storage; hydrogen desorption

1. Introduction

Our modern-day society largely depends on fossil fuels as a main energy source. The continued use of these non-renewable resources raises concerns about their sustainability as well as the environmental impact of burning these fossil fuels. Carbon dioxide, a major byproduct of the combustion of fossil fuels, is a greenhouse gas causing a rise in Earth's surface temperature [1]. In addition to climate change for future generations, burning fossil fuels can lead to health problems in the current population, such as cardiovascular and respiratory diseases [2].

The desire to reduce our current dependence on fossil fuels has led to interest in developing different clean alternative energy sources. Hydrogen has become an attractive alternative fuel candidate with a high energy density. In addition, water is the main byproduct of burning hydrogen gas. However, many challenges need to be overcome for hydrogen to be an efficient replacement for fossil fuels. One issue is that molecular hydrogen exists as a gas under ambient conditions, which has low particle density and leads to special safety and handling issues. Liquid hydrogen requires extremely low temperatures and high pressures [3]. However, solid compounds containing hydrogen are a plausible option for a safer and more efficient hydrogen storage material. Metal hydrides, in particular, have come to the forefront as a possible solid hydrogen storage material, as they can be handled more safely and are a practical alternative to other forms of hydrogen [4–13].

Magnesium hydrides have several advantages as a potential solid-state hydrogen storage metal hydride. For example, magnesium is abundant, relatively inexpensive, nontoxic, and lightweight, with a low molar mass [4,14–17]. Although the strong Mg-H bonding interactions lead to poor hydrogen sorption kinetics and thermodynamics in the solid, the hydrogen storage capacity and hydrogen sorption kinetics in magnesium hydrides

have been noted to greatly improve by doping it with transition metals [18–29]. Titanium in particular is an attractive catalytic dopant in magnesium hydride systems [21,27]. $Mg_xTi_yH_z$ systems of various compositions, for example, have shown to exhibit better (de)hydrogenation energetics and kinetics than both magnesium and titanium hydrides individually, and the hydrogen from some $Mg_xTi_yH_z$ materials has been noted to be released from the solid at lower desorption temperatures than other solids [30,31]. However, much is still not fully understood about transition metal-doped magnesium hydrides, including the role of the metal dopant, the required and optimal dopant concentration, and specific details about the desorption mechanism. However, it has been suggested that the dopant atom migrates in the material when hydrogen is released and that the magnesium–metal interactions are critically important during the release of this molecular hydrogen [22–27,32,33]. To study real-world bulk processes in greater detail, small atomic clusters are frequently used as convenient models [34–36].

Recently, we have investigated small scandium–magnesium hydride clusters, i.e., $MgScH_n$ (n = 1–20), enhancing and extending the work of prior research [37]. It was noted in this investigation that these clusters became saturated at $MgScH_{13}$ with a 15.9% hydrogen by mass, and that larger clusters contained dissociated H_2 molecules. This dissociation was proposed to occur through a weakly bound H_2 molecule coordinated to a negatively charged hydrogen atom on the cluster. Here, we investigate the impact of incorporating a different transition metal on the cluster properties, i.e., $MgTiH_n$ clusters in the same size range. This has significant importance due, in part, to the increased (de)hydrogen kinetics and energetics noted when titanium is used as a dopant in various magnesium hydride systems [21,27,30,31]. The major goals of this investigation are to explore what the hydrogen saturation size limit is for this cluster system and if it changes based on the dopant atom; to determine what the role of a different transition metal atom, specifically titanium, plays in the dissociation pathway and the preferred cluster structures; and to investigate the similarities and differences in cluster energetics and electronics with different dopant transition metal atoms as a function of increasing size.

2. Computational Methods

Candidate cluster isomers were generated using the unbiased Artificial Bee Colony algorithm implemented in the ABCluster global optimization program, were taken from previous predictions reported in the literature, or were created from our prior knowledge of likely candidate atomic cluster structures [37–40]. This ensured that both logical structures would be considered and that other candidate isomers would be located without using prior knowledge or bias. Low-energy isomers generated from the global optimization procedure, along with the additional structural isomers created for each size, were reoptimized without symmetry constraints using stringent convergence criteria via the B3PW91 density functional theory method and the 6-311++G(d,p) basis set for all atoms [41–44]. The Gaussian 16 quantum chemical package was used for all calculations [45]. This method was chosen to allow for comparison with the analogous $MgScH_n$ system studied previously at this level of theory [37]. Additionally, this theoretical approach has been shown to accurately reproduce various experimental paraments and produce the same major conclusions as higher-level ab initio methods for similar systems, and has performed better than other combinations of DFT methods and basis sets for these test cases [37]. Vibrational frequencies were calculated for each isomer to ensure that true minima structures were located. Zero-point energy corrections were included for all relative energy comparisons. All global minima isomers reported adapted the lowest possible spin multiplicity for the particular system (i.e., either singlet or doublet states depending on the number of electrons involved for the respective size). Natural Bond Orbital (NBO) analyses were performed using the NBO 7.0 program to gain further insight into the electronic and bonding properties of each cluster [46]. All calculations were performed using the Expanse high-performance computing cluster housed at the San Diego Supercomputing Center (SDSC) through the NSF-ACCESS program. Visualization of the results and pictures of each structure and the

frontier molecular orbitals were generated locally using the GaussView 6 program [47]. By exploring small $MgTiH_n$ clusters in detail here, the results will provide insight and further motivation for utilizing titanium-doped magnesium hydride solids as hydrogen storage materials.

3. Results and Discussion

3.1. Geometric Structure Determination, Growth, and Electronic Properties

For each $MgTiH_n$ size (n = 1–20), the energies of multiple isomers were compared to determine the ground state structure. As two representative examples, five low-energy local minima structures located for $MgTiH_8$ and $MgTiH_{13}$ are shown in Figure 1. The energy of each isomer in Figure 1 is reported relative to the lowest-energy isomer for that size. The lowest-energy isomers $MgTiH_8$-A and $MgTiH_{13}$-A lie over 21 kJ/mol lower in energy than structures with a single dissociated H_2 molecule (i.e., isomers $MgTiH_8$-E and $MgTiH_{13}$-B), and dissociation of additional H_2 molecules leads to even higher energy geometries for these sizes (i.e., $MgTiH_{13}$-C and $MgTiH_{13}$-E are 41.6 and 57.5 kJ/mol higher in energy than $MgTiH_{13}$-A, respectively). Note that the global minima isomers $MgTiH_8$-A and $MgTiH_{13}$-A contain an H-Mg(μ-H)$_3$Ti subunit to their structure. Isomers without this (μ-H)$_3$ group (i.e., $MgTiH_8$-D and $MgTiH_{13}$-D) lie higher in energy, and more is discussed about this particular group while discussing the growth pattern in the next paragraphs. Note also that $MgTiH_8$-A is a different lowest-energy structural isomer than what was predicted for this size when Sc was used as a transition metal (i.e., isomer $MgTiH_8$-C is analogous to the global minimum $MgScH_8$ isomer reported previously [37]), and, interestingly, structural changes based on transition metal dopant identity can already be noted. A more detailed discussion of the relationship between $MgTiH_n$ and $MgScH_n$ clusters is presented later in Section 3.2. Calculations were also performed at the B3PW91/lanl2dz level, and they gave similar results. At this B3PW91/lanl2dz level of theory, $MgTiH_8$-A was also predicted to be the lowest-energy $MgTiH_8$ structure, lying 6.6 kJ/mol lower in energy than $MgTiH_8$-B. Interestingly, at this level, $MgTiH_8$-E with a dissociated H_2 unit lay only 7.8 kJ/mol higher in energy than the global minima $MgTiH_8$-A structure.
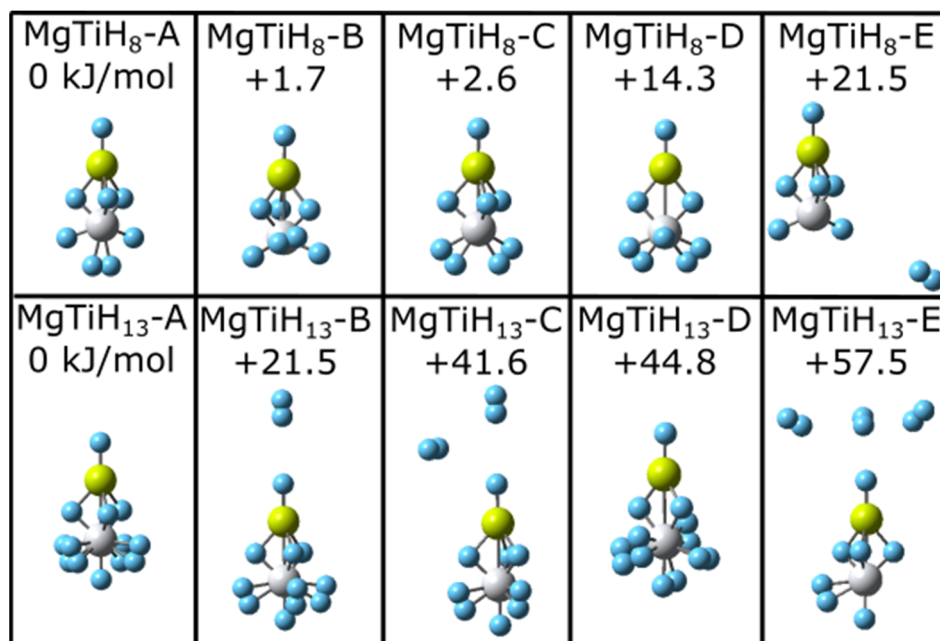

Figure 1. Low-energy structural isomers of $MgTiH_8$ (**top**) and $MgTiH_{13}$ (**bottom**). For each structure, magnesium atoms are colored yellow, titanium atoms are grey, and hydrogen atoms are blue. Relative energy values are listed in kJ/mol.

The ground state structures and frontier molecular orbitals of all of the lowest-energy MgTiH$_n$ isomers located for n = 1–12 and n = 13–20 are shown in Figures 2 and 3, respectively. The coordinates of all of the located global minima isomers in standard xyz format are provided in the Supporting Information for this article. For small-sized MgTiH$_1$–MgTiH$_4$, hydrogen atoms either bind to the Ti center or act as bridging hydrogen atoms between titanium and magnesium. When an odd number of hydrogen atoms is present for these small sizes (i.e., for the MgTiH and MgTiH$_3$ doublet species), hydrogen atoms bind exclusively as bridge-bound hydrogens. However, when an even number of hydrogen atoms are present (i.e., for the MgTiH$_2$ and MgTiH$_4$ singlet species), two hydrogen atoms bind to the titanium center. For MgTiH$_5$, a single hydrogen atom binds solely to Mg, and three bridge-bonded hydrogen atoms exist. Once this H-Mg(μ-H)$_3$Ti entity is formed in MgTiH$_5$, the group also exists as a structural motif in the ground state geometry for all larger-sized clusters in the size range explored here. For MgTiH$_6$–MgTiH$_{14}$, hydrogen atoms continue to bind to the titanium center either as H atoms or as molecular H$_2$. For MgTiH$_{15}$ and larger cluster sizes, weakly interacting H$_2$ molecule(s) are dissociated from the MgTiH$_{13}$ or MgTiH$_{14}$ cluster core, depending on whether an odd or even number of hydrogen atoms is present, respectively. This MgTiH$_{14}$ size thus sets the hydrogen saturation limit on these clusters, indicating a maximum hydrogen capacity of 16.4% by mass in the MgTiH$_n$ system.
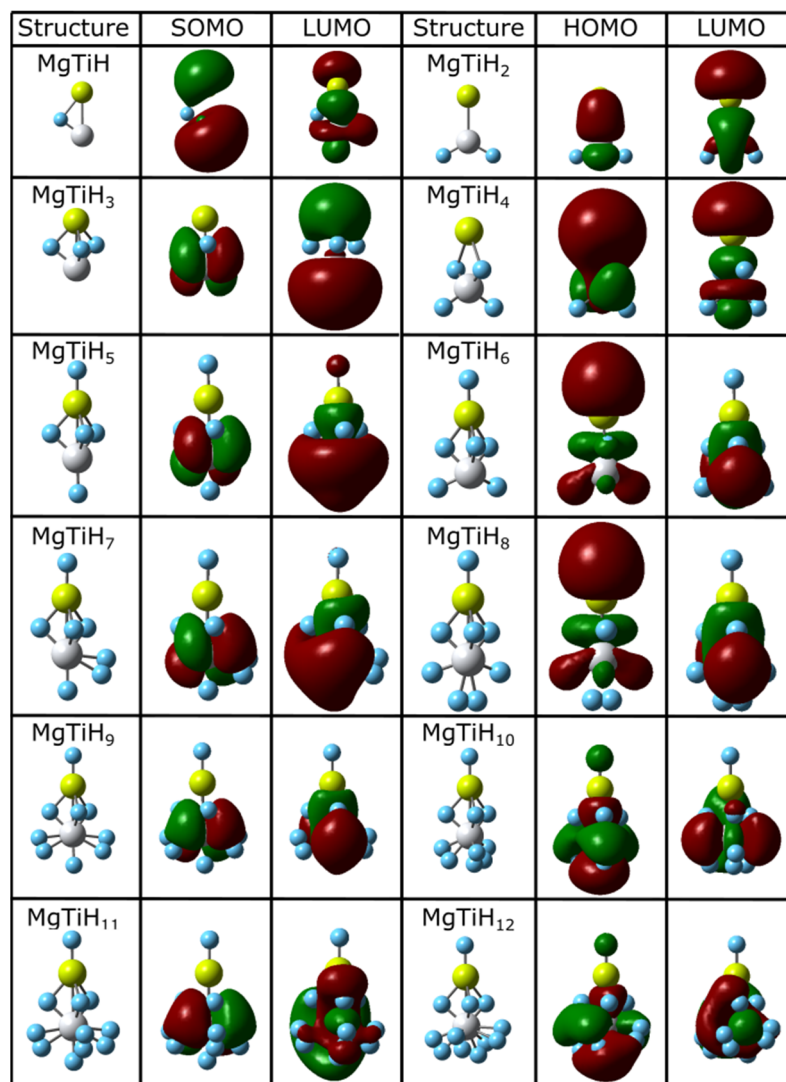

Figure 2. Lowest-energy isomers and frontier orbitals of MgTiH$_n$ (n = 1–12). For each structure, magnesium atoms are colored yellow, titanium atoms are grey, and hydrogen atoms are blue.

Structure	SOMO	LUMO	Structure	HOMO	LUMO
MgTiH$_{13}$			MgTiH$_{14}$		
MgTiH$_{15}$			MgTiH$_{16}$		
MgTiH$_{17}$			MgTiH$_{18}$		
MgTiH$_{19}$			MgTiH$_{20}$		

Figure 3. Lowest-energy isomers and frontier orbitals of MgTiH$_n$ (n = 13–20). For each structure, magnesium atoms are colored yellow, titanium atoms are grey, and hydrogen atoms are blue.
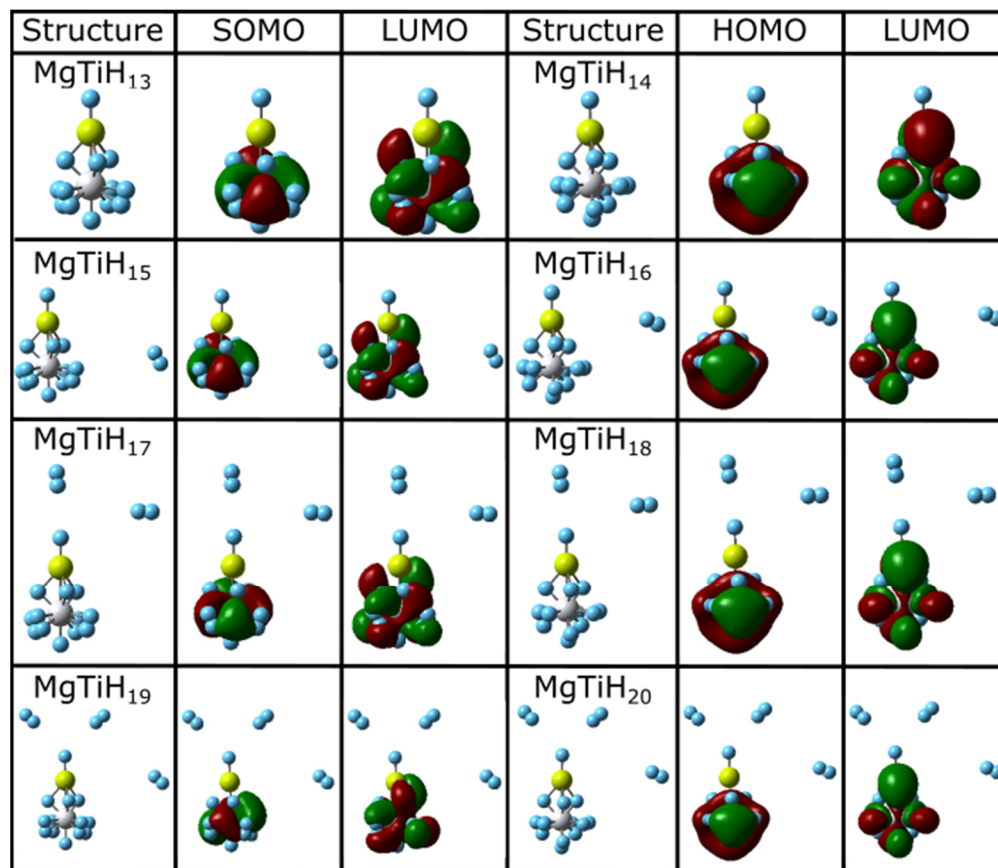
Once H$_2$ dissociation occurs for MgTiH$_n$ ($n \geq 15$), the weakly bound H$_2$ molecule appears at different locations in the ground state structure. After the first H$_2$ molecule in MgTiH$_{15}$ and MgTiH$_{16}$ appears along the cluster's side, additional H$_2$ molecules in MgTiH$_n$ (n = 17–20) aggregate oriented along the Ti-Mg-H backbone of the cluster. A similar observation was noted in MgScH$_n$ clusters [37]. This provides further evidence that dihydrogen may prefer to dissociate through coordinating with the metal-Mg-H backbone, particularly after the first H$_2$ molecule dissociates. It seems likely the transition metal may aid in the release of dihydrogen from magnesium hydrides solids as the transition metal diffuses into the solid. By doing so, this may lead to a hydride with a large negative partial charge that dissociated dihydrogen can coordinate to with a temporary dipole. For example, in the ground state structure of MgTiH$_{17}$, NBO charges indicate the partial charges for each atom along the Ti-Mg-H backbone to be -0.399, $+1.482$, and -0.654, respectively. The dissociated dihydrogen aligned with this backbone has a temporary dipole with partial charges on the two hydrogen atoms of $+0.014$ and -0.015. Hence, the dissociated H$_2$ molecule is able to weakly interact with the large, negatively charged hydride (-0.654) in the cluster, which may aid in stabilizing the H$_2$ as it dissociates from metal-doped magnesium hydride materials.

The highest occupied molecular orbital (HOMO) and lowest unoccupied molecular orbital (LUMO), which jointly make up the frontier orbitals for these clusters, are also shown in Figures 2 and 3. These orbitals primarily consist of magnesium *p* and titanium *d* character. This is easily seen for smaller-sized clusters, and the frontier orbitals become increasingly complicated as the cluster size increases. For example, in the MgTiH$_2$ cluster, the *p* and *d* orbitals of Mg and Ti, respectively, overlap constructively in these frontier orbitals. For doublet species with an odd number of electrons, the singly occupied molecule orbital (SOMO) is denoted for the HOMO, as is common, and is more descriptive for

the system. Figures 2 and 3 show clusters with an odd number of hydrogen (doublet systems) on the left side and clusters with an even number of hydrogen atoms (singlet systems) on the right. Thus, similarities can be noted down a column, and the HOMO and SOMO are labeled accordingly for a given column. Note, for example, that once a cluster is saturated with hydrogen atoms (i.e., for $MgTiH_{13}$ and $MgTiH_{14}$), the addition of dissociated H_2 molecules for larger $MgTiH_n$ ($n \geq 15$) clusters does not change the frontier orbitals significantly.

Table 1 presents the natural electron configurations (NECs) for magnesium and titanium atoms in $MgTiH_n$ ($n = 1\text{–}20$) ground state clusters. It also includes the Mullikan and natural partial charges for both metal atoms in each structure. The NECs show that titanium predominantly loses s electron density and gains d character in the cluster relative to the atomic electron configuration, whereas magnesium predominantly loses s electron density. In general, Mullikan and natural partial charges have the same sign for each metal in the cluster, but natural charges are typically predicted to be larger in magnitude for both metals. This is a similar trend to what was observed for $MgScH_n$ clusters [37]. While the partial charge of Mg is predicted to be positively charged for every ground state structure, titanium is positively charged for small-sized clusters and becomes partially negatively charged in $MgTiH_{12}$ and larger sizes. At $n = 5$ and larger, the natural charge on magnesium remains relatively constant up to $n = 20$.

Table 1. The natural electron configuration (NEC), Mullikan charges, and natural charges for the metal atoms in $MgTiH_n$ ($n = 1\text{–}20$) clusters.

H Atoms (n)	NEC	Mullikan Charge (Mg/Ti)	Natural Charge (Mg/Ti)
1	$Mg{:}3s^{1.68}3p^{0.04}5s^{0.01}$ $Ti{:}4s^{1.03}3d^{2.59}4p^{0.06}4d^{0.01}$	0.146/0.0469	0.265/0.303
2	$Mg{:}3s^{1.68}3p^{0.06}$ $Ti{:}4s^{0.53}3d^{2.61}4p^{0.13}4d^{0.01}$	0.147/0.336	0.253/0.711
3	$Mg{:}3s^{0.99}3p^{0.06}4s^{0.01}3d^{0.01}$ $Ti{:}4s^{0.38}3d^{2.80}4p^{0.03}5s^{0.01}4d^{0.01}$	0.374/0.532	0.921/0.774
4	$Mg{:}3s^{1.53}3p^{0.01}4s^{0.01}$ $Ti{:}4s^{0.64}3d^{2.32}4p^{0.07}4d^{0.01}$	0.290/0.617	0.449/0.961
5	$Mg{:}3s^{0.53}3d^{0.01}5p^{0.04}$ $Ti{:}4s^{0.37}3d^{2.39}4p^{0.03}4d^{0.02}$	0.831/0.456	1.422/1.179
6	$Mg{:}3s^{0.51}5p^{0.05}$ $Ti{:}4s^{0.45}3d^{2.58}4p^{0.04}4d^{0.02}$	0.602/0.513	1.437/0.911
7	$Mg{:}3s^{0.51}4p^{0.04}$ $Ti{:}4s^{0.37}3d^{2.72}4p^{0.02}4d^{0.03}$	0.783/0.324	1.437/0.861
8	$Mg{:}3s^{0.50}3p^{0.04}$ $Ti{:}4s^{0.41}3d^{3.05}4p^{0.02}4d^{0.03}$	0.683/0.244	1.454/0.484
9	$Mg{:}3s^{0.50}5p^{0.04}$ $Ti{:}4s^{0.36}3d^{3.09}4p^{0.02}4d^{0.04}$	0.724/0.144	1.451/0.490
10	$Mg{:}3s^{0.50}3p^{0.04}$ $Ti{:}4s^{0.37}3d^{3.58}4p^{0.01}4d^{0.02}$	0.670/−0.036	1.459/0.011
11	$Mg{:}3s^{0.49}6p^{0.04}$ $Ti{:}4s^{0.36}3d^{3.53}4p^{0.02}4d^{0.05}$	0.689/−0.0699	1.467/0.039

Table 1. *Cont.*

H Atoms (*n*)	NEC	Mullikan Charge (Mg/Ti)	Natural Charge (Mg/Ti)
12	Mg:$3s^{0.49}6p^{0.04}$ / Ti:$4s^{0.37}3d^{3.97}4d^{0.02}5p^{0.02}$	$0.566/-0.0458$	$1.467/-0.379$
13	Mg:$3s^{0.48}6p^{0.04}$ / Ti:$3d^{3.95}4p^{0.02}5s^{0.38}4d^{0.05}$	$0.607/-0.247$	$1.476/-0.399$
14	Mg:$3s^{0.47}6p^{0.04}$ / Ti:$4s^{0.36}3d^{4.62}4d^{0.01}5p^{0.01}$	$0.547/-0.584$	$1.482/-1.013$
15	Mg:$3s^{0.48}6p^{0.04}$ / Ti:$3d^{3.95}4p^{0.02}5s^{0.38}4d^{0.05}$	$0.608/-0.248$	$1.475/-0.400$
16	Mg:$3s^{0.47}5p^{0.04}$ / Ti:$4s^{0.36}3d^{4.62}4d^{0.01}5p^{0.01}$	$0.547/-0.581$	$1.481/-1.013$
17	Mg:$3s^{0.48}5p^{0.04}$ / Ti:$4s^{0.38}3d^{3.95}4p^{0.02}4d^{0.05}$	$0.539/-0.122$	$1.482/-0.399$
18	Mg:$3s^{0.47}6p^{0.04}$ / Ti:$4s^{0.36}3d^{4.62}4d^{0.01}5p^{0.01}$	$0.457/-0.433$	$1.487/-1.012$
19	Mg:$3s^{0.47}5p^{0.04}$ / Ti:$4s^{0.38}3d^{3.95}4p^{0.02}4d^{0.05}$	$0.576/-0.195$	$1.482/-0.399$
20	Mg:$3s^{0.47}4p^{0.04}$ / Ti:$3d^{4.62}5s^{0.36}4d^{0.01}5p^{0.01}$	$0.522/-0.551$	$1.488/-1.012$

3.2. MgTiH$_n$ and MgScH$_n$ Comparison

In comparing the ground state structures of MgTiH$_n$ clusters assigned in the previous section and MgScH$_n$ reported previously [37], several interesting observations can be noted. First, the lowest-energy isomer of the small MgTiH$_8$ cluster contains a TiH$_2$(H$_2$) group (i.e., two hydrogen atoms and an H$_2$ molecule bound to Ti). This differs from the ground state of MgScH$_8$, where a Sc(H$_2$)$_2$ group exists. The reported HMg(μ-H)$_3$TiH$_2$(H$_2$) ground state structure of MgTiH$_8$ lies 2.6 kJ/mol lower in energy than a possible HMg(μ-H)$_3$Ti(H$_2$)$_2$ structure (which is the lowest-energy Sc isomer) at this level of theory. This preference for two hydrogen atoms and a hydrogen molecule bound to the metal, rather than two diatomic hydrogen molecules, likely arises from the presence of an additional electron on the Ti center compared to Sc. This difference is also important, as it impacts various parameters of the clusters. For example, the presence of terminal hydrogen atoms, as opposed to hydrogen molecules, bound to the metal has an impact on the metal–magnesium bond length. This is discussed in more detail in Section 3.3. Secondly, all hydrogen atoms remain bound to the lowest-energy MgTiH$_{14}$ cluster, and MgTiH$_{15}$ is the first size cluster with a dissociated H$_2$ molecule. Hence, MgTiH$_{14}$ achieves hydrogen saturation, and the maximum hydrogen capacity of this system is found to be 16.4% by mass. This is larger and differs from the analogous scandium system where MgScH$_{13}$, which is 15.9% hydrogen by mass, is the largest cluster without a dissociated H$_2$ molecule. This hydrogen dissociation at different-sized clusters for two transition metals that differ in their number of valence electrons but have similar sizes implies, at least in part, that dissociation likely occurs due to the electronic properties of the transition metal dopant rather than steric factors.

3.3. Cluster Stability and Energetics

In the discussion on cluster energetics here, we focus mainly on trends that are predicted rather than absolute values at this level of theory employed. Figure 4 shows the

absolute value of the HOMO-LUMO energy gap as a function of the number of hydrogen atoms in a cluster. For doublet electronic species (i.e., species with an odd number of hydrogen atoms), the singly occupied molecular orbital (SOMO) is taken as the HOMO. This energy gap, while it should only be taken as qualitative at this level of theory, provides a relative indication of the inertness or reactivity of a specific cluster, with a higher energy gap indicating a more inert cluster. In Figure 4, it is seen that the HOMO-LUMO gap generally increases with size up to $MgTiH_{13}$; is the largest for $MgTiH_n$ ($n \geq 13$), where the clusters are predicted to be the most inert in this cluster size range; and remains fairly constant for larger sizes. This is appropriate, as H_2 molecules begin to dissociate from the saturated clusters at this size and the general cluster structure remains relatively constant with each additional dissociated hydrogen molecule. Note that this maximum gap energy is only slightly less than the maximum calculated for $MgScH_n$ clusters [37].
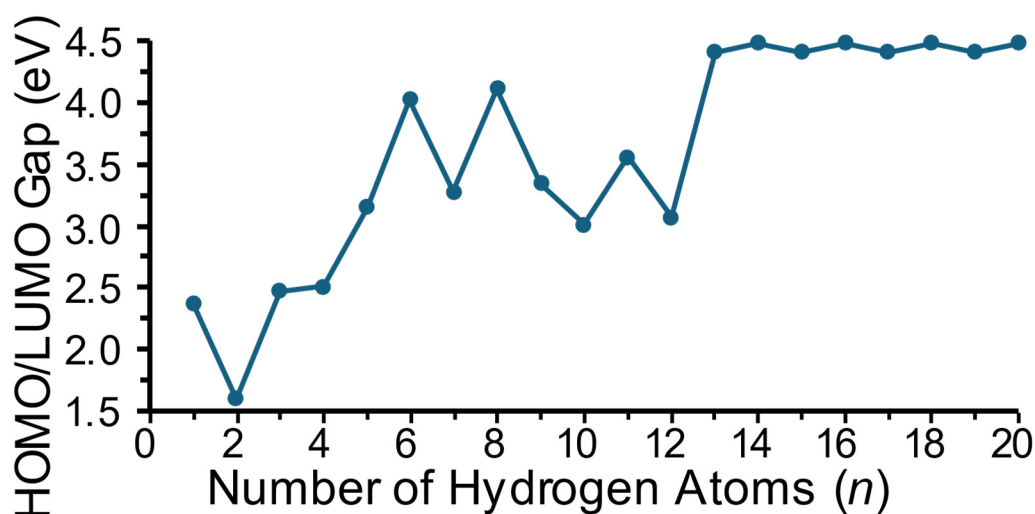

Figure 4. Frontier molecular orbital energy gap as a function of the number of hydrogen atoms in $MgTiH_n$ clusters.

Figure 5 shows the magnesium–titanium bond length as a function of the number of hydrogen atoms in the cluster. The magnesium–titanium bond length changes for the smaller $MgTiH_n$ ($n = 1$–5) size range, but varies to a lesser degree when n is greater than 5. For $MgTiH_{13}$ and larger sizes, once hydrogen saturation occurs in the $MgTiH_n$ cluster, the Mg-Ti distance remains relatively constant. Note that $MgTiH$, $MgTiH_2$, and $MgTiH_4$, which have the longest predicted Mg-Ti bond lengths of 2.867, 2.813, and 2.880 Å, respectively, correspond to the three sized clusters where the ground state structure does not possess a full three-hydrogen-atom bridge-bound $Mg(\mu\text{-}H)_3Ti$ unit. $MgTiH_3$, which has the shortest Mg-Ti bond length of 2.564 Å, contains a full $Mg(\mu\text{-}H)_3Ti$ group without any additional terminal hydrogen atoms in the cluster, and these bridging hydrogen atoms appear to lead to structures with shorter Mg-Ti distances. For $MgTiH_{10}$ and $MgTiH_{12}$, there is also a decreased Mg-Ti bond length compared to other clusters in this size range, although to a lesser extent than that seen for smaller sized clusters. Similarly to $MgTiH_3$, $MgTiH_{10}$ and $MgTiH_{12}$ do not contain any terminal Ti-H bonds (i.e., all of the hydrogen atoms bound to Ti are either as H_2 units or bridge bound $Mg(\mu\text{-}H)_3Ti$). Hence, the decreased Mg-Ti length appears to be due to the cluster containing the three bridge-bound hydrogen atoms, without any additional terminal H atoms bound to the titanium center.
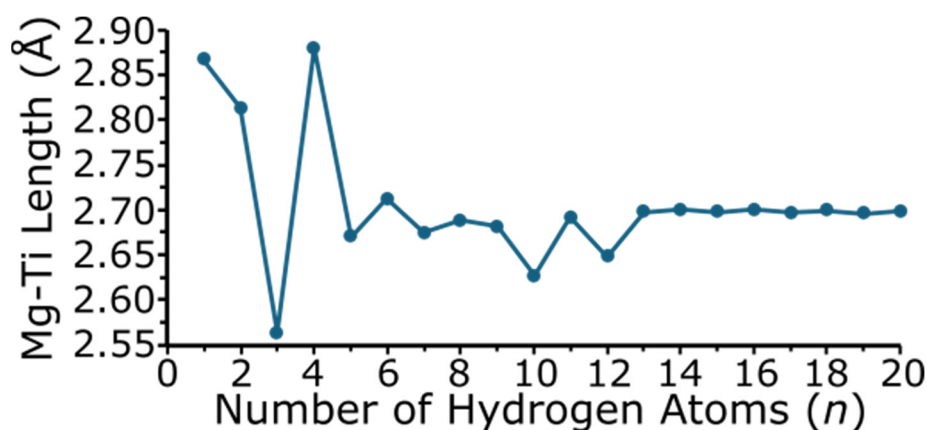
Figure 5. Bond length between magnesium and titanium as a function of the number of hydrogen atoms in each MgTiH$_n$ cluster.

Figure 6 shows the binding energy (E$_{bind}$) of the MgTiH$_n$ clusters. The binding energy, or fragmentation energy, is calculated by Equation (1) and is the sum of the energy of each individual atom making up the MgTiH$_n$ cluster minus the energy of the cluster, and is normalized for the total number of atoms in the cluster by dividing by $n + 2$.

$$E_{bind}(n) = \frac{E_{Mg} + E_{Ti} + nE_H - E_{MgTiH_n}}{n + 2} \tag{1}$$
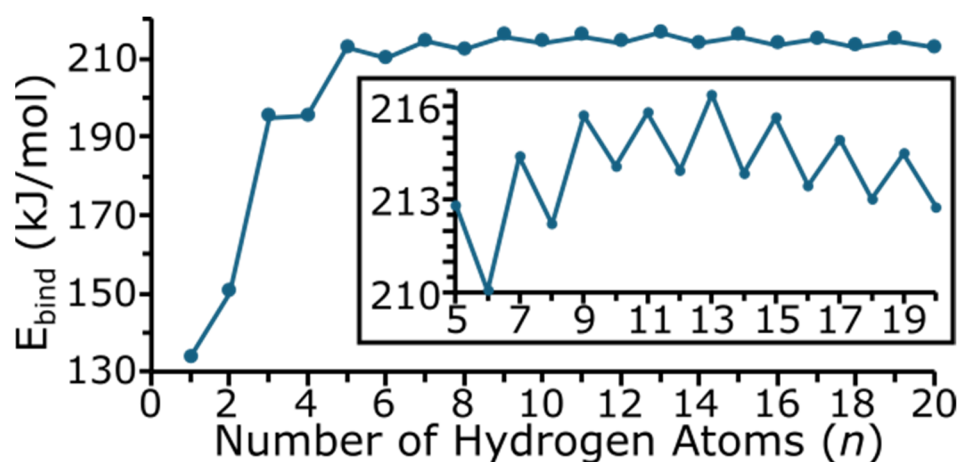
Figure 6. Binding (fragmentation) energy as a function of the number of hydrogen atoms in MgTiH$_n$ clusters (n = 1–20). The insert shows a blown-up portion of the overall plot for n = 5–20.

Hence, a more positive E$_{bind}$ value denotes a more stable cluster, and as all of the E$_{bind}$ values are positive, this indicates that the clusters studied here are more stable than the individual atoms making up the cluster. The numerical values of E$_{bind}$ are given in the Supporting Information. As expected, the E$_{bind}$ of the cluster increases drastically as n increases for small-sized clusters, and then begins to level off and change more gradually for larger-sized clusters. The odd/even oscillation seen in Figure 6 indicates that clusters with an odd number of hydrogen atoms are, in general, more stable for this system. A larger blown-up section for n = 5–20 is shown as an insert in Figure 6. In this region, note that the energy increases up to n = 13, and then begins to decrease. Hence, MgTiH$_{13}$ appears to be a more stable cluster size with regard to E$_{bind}$. For clusters with an even number of hydrogen atoms, the E$_{bind}$ increases up to MgTiH$_{10}$ and then begins to decrease with cluster size.

The relative stability of each cluster compares the energy of a cluster in relationship to its neighboring-sized clusters with one more and one less hydrogen atom (or two more

and two less hydrogen atoms). These E_{stab1} and E_{stab2} relative energies are calculated using Equations (2) and (3), respectively.

$$E_{stab1}\ (n) = 2E_{MgTiH_n} - E_{MgTiH_{n-1}} - E_{MgTiH_{n+1}} \tag{2}$$

$$E_{stab2}\ (n) = 2E_{MgTiH_n} - E_{MgTiH_{n-2}} - E_{MgTiH_{n+2}} \tag{3}$$

Figure 7 depicts E_{stab1} and E_{stab2} as functions of cluster size and each are additional metrics to indicate the relative stability of each cluster. As these are calculated with Equations (2) and (3), a more negative stabilization energy indicates an enhanced stability relative to its neighboring-sized clusters. The numerical values of E_{stab1} and E_{stab2} are also provided in Table S1 of the Supporting Information. With E_{stab1}, an odd/even oscillation can be seen, which again indicates that clusters with an odd number of hydrogen atoms are more stable than their even-numbered neighbors. For clusters with an odd number of hydrogen atoms, we again note that $MgTiH_{13}$ is more stable (i.e., has a more a negative E_{stab1}) than other clusters similar in size. For even-numbered hydrogens, we note that $MgTiH_{10}$ is a minimum, and E_{stab1} indicates that this size is more stable than other $MgTiH_n$ clusters with an even number of hydrogen atoms. While E_{stab2} compares clusters with a similar odd or even number of hydrogen atoms, it also compares clusters that vary more in size, differing by two hydrogen atoms. However, E_{stab2} again indicates that, in addition to small $MgTiH_n$ clusters, $MgTiH_{10}$ and $MgTiH_{13}$ are more stable larger species than other clusters in this size range. As expected, E_{stab2} does not vary significantly once hydrogen saturation and dissociation occur for the largest clusters studies here.
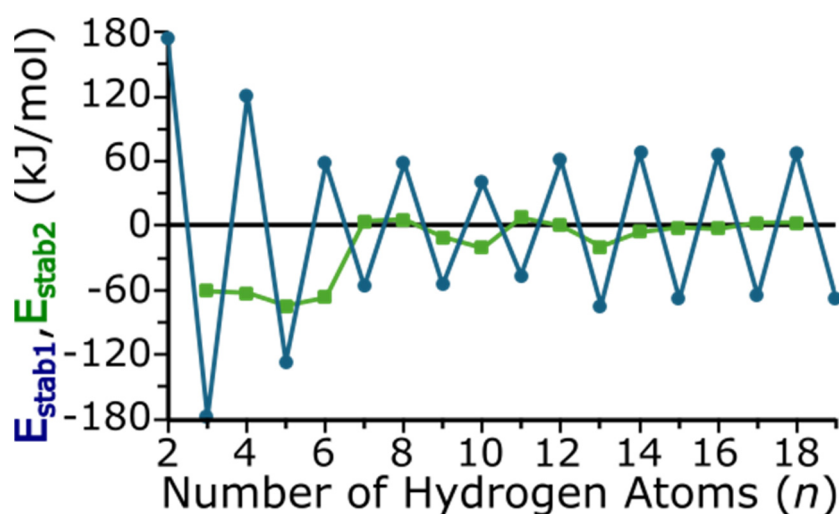

Figure 7. Relative energy between $MgTiH_n$ clusters as a function of the number of hydrogen atoms per cluster. E_{stab1} (blue circles) compares the energy of a cluster with that containing one more and less hydrogen atom, whereas E_{stab2} (green squares) compares the energy of a cluster with that containing two more and less hydrogen atoms. See text for additional details.

4. Conclusions

In summary, we have explored the structures, growth mechanism, stability, and energetics of $MgTiH_n$ ($n \leq 20$) clusters at the B3PW91 hybrid density functional level of theory with an all-electron 6-311++G(d,p) basis set for all atoms. We have shown that hydrogen atoms predominantly bind to titanium in small $MgTiH_n$ clusters. Additionally, hydrogen saturation occurs at $MgTiH_{14}$ with a large 16.4% hydrogen by mass, and clusters with an odd number of hydrogen atoms are more stable than those with an even number of hydrogen atoms. Particularly, $MgTiH_{10}$ and $MgTiH_{13}$ are more stable clusters with even and odd numbers of hydrogen atoms, respectively. The cluster frontier orbitals are primarily made up of magnesium *p* and titanium *d* atomic orbitals. A plausible mechanism for H_2 dissociation from metal-doped magnesium hydride solids, which is supported by

NBO analysis in MgTiH$_n$ clusters, is described where H$_2$ molecules desorb while weakly interacting with an anionic hydride in the solid. In the desorption process, the anionic hydride forms a weak intermolecular interaction with a temporary dipole of the dissociating H$_2$ molecule.

Author Contributions: Conceptualization, J.T.L.; methodology, C.N., D.B., and J.T.L.; validation, C.N., D.B., and J.T.L.; formal analysis, C.N. and J.T.L.; investigation, C.N. and J.T.L.; resources, J.T.L.; data curation, C.N. and J.T.L.; writing—original draft preparation, C.N. and J.T.L.; writing—review and editing, J.T.L.; visualization, C.N. and J.T.L.; supervision, D.B. and J.T.L.; project administration, C.N., D.B., and J.T.L.; funding acquisition, J.T.L. All authors have read and agreed to the published version of the manuscript.

Data Availability Statement: The Cartesian coordinates of the optimized global minimum structures for each size are available in standard xyz format in the Supplementary Materials.

Conflicts of Interest: The authors declare no conflicts of interest.

References

1. Solomon, C.G.; Salas, R.N.; Malina, D.; Sacks, C.A.; Hardin, C.C.; Prewitt, E.; Lee, T.H.; Rubin, E.J. Fossil-Fuel Pollution and Climate Change—A New Nejm Group Series. *N. Engl. J. Med.* **2022**, *386*, 2328–2329. [CrossRef] [PubMed]
2. Koch, S.; Klitzman, R. Reliance on Fossil Fuels: Ethical Implications for Intensivists. *Intensive Care Med.* **2023**, *49*, 330–333. [CrossRef] [PubMed]
3. Zhang, Y.; Jia, Z.; Yuan, Z.; Yang, T.; Qi, Y.; Zhao, D. Development and Application of Hydrogen Storage. *J. Iron Steel Res. Int.* **2015**, *22*, 757–770. [CrossRef]
4. Yartys, V.A.; Lototskyy, M.V.; Akiba, E.; Albert, R.; Antonov, V.E.; Ares, J.R.; Baricco, M.; Bourgeois, N.; Buckley, C.E.; Bellosta von Colbe, J.M.; et al. Magnesium based materials for hydrogen based storage: Past, present, and future. *Int. J. Hydrogen Energy* **2019**, *44*, 7809–7859. [CrossRef]
5. von Colbe, J.B.; Ares, J.-R.; Barale, J.; Baricco, M.; Buckley, C.; Capurso, G.; Galladat, N.; Grant, D.M.; Guzik, M.N.; Jacob, I.; et al. Application of hydrides in hydrogen storage and compression: Achievements, outlook and perspectives. *Int. J. Hydrogen Energy* **2019**, *44*, 7780–7808. [CrossRef]
6. Zhou, W.; Jin, S.; Dai, W.; Lyon, J.T.; Lu, C. Theoretical study on the structural evolution and hydrogen storage in NbHn (n = 2–15) clusters. *Int. J. Hydrogen Energy* **2021**, *46*, 17246–17252. [CrossRef]
7. Liao, Y.H.; Zhou, W.L.; Lyon, J.T.; Peng, F.; Lu, C. The structure of anionic NbH$_n^-$ (n = 2–15) clusters and their maximum hydrogen capacity. *New J. Phys.* **2022**, *24*, 043038. [CrossRef]
8. Schneemann, A.; White, J.L.; Kang, S.; Jeong, S.; Wan, L.F.; Cho, E.S.; Heo, T.W.; Prendergast, D.; Urban, J.J.; Wood, B.C.; et al. Nanostructure Metal Hydrides for Hydrogen Storage. *Chem. Rev.* **2018**, *118*, 10775–10839. [CrossRef]
9. Dragassi, M.-C.; Royon, L.; Redolfi, M.; Ammar, S. Hydrogen Storage as a Key Energy Vector for Car Transportation: A Tutorial Review. *Hydrogen* **2023**, *4*, 831–861. [CrossRef]
10. Lobo, R.F.M. A Brief on Nano-Based Hydrogen Energy Transition. *Hydrogen* **2023**, *4*, 679–693. [CrossRef]
11. Fiorio, J.L.; Goethe, M.L.; Kohlrausch, E.C.; Zardo, M.L.; Tanaka, A.A.; de Lima, R.B.; da Silva, A.G.M.; Garcia, M.A.S.; Vidinha, P.; Machado, G. Nanoengineering of Catalysts for Enhanced Hydrogen Production. *Hydrogen* **2022**, *3*, 218–254. [CrossRef]
12. Pistidda, C. Solid-State Hydrogen Storage for a Decarbonized Society. *Hydrogen* **2021**, *2*, 428–443. [CrossRef]

13. Cao, Z.; Habermann, F.; Burkmann, K.; Felderhoff, M.; Mertens, F. Unstable Metal Hydrides for Possible On-Board Hydrogen Storage. *Hydrogen* **2024**, *5*, 241–279. [CrossRef]

14. Vajeeston, P.; Ravindran, P.; Fjellvåg, H. Predicting New Materials for Hydrogen Storage Application. *Materials* **2009**, *2*, 2296–2318. [CrossRef]

15. Zhang, J.; Li, J.; Wu, Y.; Guo, X.; Ye, J.; Yuan, B.; Wang, S.; Jiang, L. Recent advances on the thermal destabilization of Mg-based hydrogen storage materials. *RSC Adv.* **2019**, *9*, 408–428. [CrossRef] [PubMed]

16. Hevia, E.; Mulvey, R.E. A Record-Breaking Magnesium Hydride Molecular Cluster: Implications for Hydrogen Storage. *Angew. Chem. Int. Ed.* **2011**, *50*, 9242–9243. [CrossRef]

17. Seifert, F.; Görls, H.; Kupfer, S.; Kretschmer, R. A tetranuclear magnesium hydride cluster with a four-coordinate hydride in near square-planar geometry. *Chem. Commun.* **2023**, *59*, 7627–7630. [CrossRef]

18. Wang, Y.; Wang, Y. Recent Advances in Additive-Enhanced Magnesium Hydride for Hydrogen Storage. *Prog. Nat. Sci. Mater. Int.* **2017**, *27*, 41–49. [CrossRef]

19. Zhang, J.; Sun, L.Q.; Zhou, Y.C.; Peng, P. Dehydrogenation Thermodynamics of Magnesium Hydride Doped with Transition Metals: Experimental and Theoretical Studies. *Comput. Mater. Sci.* **2015**, *98*, 211–219. [CrossRef]

20. El Khatabi, M.; Bhihi, M.; Naji, S.; Labrim, H.; Benyoussef, A.; El Kenz, A.; Loulidi, M. Study of Doping Effects with 3d and 4d-Transition Metals on the Hydrogen Storage Properties of MgH$_2$. *Int. J. Hydrogen Energy* **2016**, *41*, 4712–4718. [CrossRef]

21. Zhou, C.; Zhang, J.; Bowman, R.C.; Fang, Z.Z. Roles of Ti-Based Catalysts on Magnesium Hydride and Its Hydrogen Storage Properties. *Inorganics* **2021**, *9*, 36. [CrossRef]

22. Larsson, P.; Araúo, C.M.; Larsson, J.A.; Jena, P.; Ahuja, R. Role of catalysts in dehydrogenation of MgH$_2$ nanoclusters. *Proc. Natl. Acad. Sci. USA* **2008**, *105*, 8227–8231. [CrossRef] [PubMed]

23. Bazzanella, N.; Checchetto, R.; Miotello, A. Atoms and Nanoparticles of Transition Metals as Catalysts for Hydrogen Desorption from Magnesium Hydride. *J. Nanomater.* **2011**, *2011*, 865969. [CrossRef]

24. Li, Q.; Yan, M.; Xu, Y.; Zhang, X.L.; Lau, K.T.; Sun, C.; Jia, B. Computational Investigation of MgH$_2$/NbOx for Hydrogen Storage. *J. Phys. Chem. C* **2021**, *125*, 8862–8868. [CrossRef]

25. Sun, Z.; Lu, X.; Nyahuma, F.M.; Yan, N.; Xiao, J.; Su, S.; Zhang, L. Enhancing Hydrogen Storage Properties of MgH$_2$ by Transition Metals and Carbon Materials: A Brief Review. *Front. Chem.* **2020**, *8*, 552. [CrossRef] [PubMed]

26. Charkin, O.P.; Maltsev, A.P. Density Functional Theory Modeling of Reactions of Addition of H$_2$ Molecules to Magnesium Clusters Mg17M Doped with Atoms M of Transition 3d Elements. *J. Phys. Chem. A* **2021**, *125*, 2308–2315. [CrossRef]

27. Jangir, M.; Jain, I.P.; Gattia, D.M. Effect of Ti-Based Additives on the Hydrogen Storage Properties of MgH$_2$: A Review. *Hydrogen* **2023**, *4*, 523–541. [CrossRef]

28. Yuan, Q.; Peng, C.; Yang, C.; Li, Y.; Zhang, Q.; Lv, Y.; Liu, G.; Liu, D. Facilitated hydrogen storage properties of MgH$_2$ by Ni nanoparticles anchored on Mo$_2$C@C nanosheets. *Int. J. Hydrogen Energy* **2024**, *85*, 12–19. [CrossRef]

29. Khandelwal, P.; Rathi, B.; Agarwal, S.; Juyal, S.; Gill, F.S.; Kumar, M.; Saini, P.; Dixit, A.; Ichikawa, T.; Jain, A. Core-shell structured Ni@C based additive for magnesium hydride system towards efficient hydrogen sorption kinetics. *Int. J. Hydrogen Energy*, 2024; *in press*. [CrossRef]

30. Er, S.; van Setten, M.J.; de Wijs, G.A.; Brocks, G. First-principles modelling of magnesium titanium hydrides. *J. Phys. Condens. Matter* **2010**, *22*, 074208. [CrossRef]

31. Kyoi, D.; Sato, T.; Rönnebro, E.; Kitamura, N.; Ueda, A.; Ito, M.; Katsuyama, S.; Hara, S.; Noréus, D.; Sakai, T. A new ternary magnesium-titanium hydride Mg7TiHx with hydrogen desorption properties better than both binary magnesium and titanium hydrides. *J. Alloys Compd.* **2004**, *372*, 213–217. [CrossRef]

32. Luo, X.; Grant, D.M.; Walker, G.S. Hydrogen storage properties of nano-structured 0.65MgH$_2$/0.35ScH$_2$. *Int. J. Hydrogen Energy* **2013**, *38*, 153–161. [CrossRef]

33. Garçon, M.; Bakewell, C.; Sackman, G.A.; White, A.J.P.; Cooper, R.I.; Edwards, A.J.; Crimmin, M.R. A hexagonal planar transition-metal complex. *Nature* **2019**, *574*, 390–393. [CrossRef] [PubMed]

34. Dore, E.M.; Lyon, J.T. The Structures of Silicon Clusters Doped with Two Gold Atoms, SinAu2 (n = 1–10). *J. Clust. Sci.* **2016**, *27*, 1365–1381. [CrossRef]

35. Lyon, J.T. Building Blocks: Investigating the Structures, Properties, and Reactivity of Strongly Bound Atomic Clusters at a PUI. In *Physical Chemistry Research at Undergraduate Institutions*; Hopkins, T., Parish, C.A., Eds.; ACS Books: Washington, DC, USA, 2022; Volume 2, Chapter 10; pp. 165–179. [CrossRef]

36. Lyon, J.T.; Gruene, P.; Fielicke, A.; Meijer, G.; Rayner, D.M. Probing C-O bond activation on gas-phase transition metal clusters: Infrared multiple photon dissociation spectroscopy of Fe, Ru, Re, and W cluster CO complexes. *J. Chem. Phys.* **2009**, *131*, 184706. [CrossRef]

37. Lyon, J.T. Hydrogen Binding and Dissociation in MgScHn Clusters (n ≤ 20). *Int. J. Hydrogen Energy* **2021**, *46*, 36872–36877. [CrossRef]

38. Zhang, J.; Dolg, M. ABCLUSTER: The Artificial Bee Colony Algorithm for Cluster Global Optimization. *Phys. Chem. Chem. Phys.* **2015**, *17*, 24173–24181. [CrossRef]

39. Zhang, J.; Dolg, M. Global Optimization of Clusters of Rigid Molecules Using the Artificial Bee Colony Algorithm. *Phys. Chem. Chem. Phys.* **2016**, *18*, 3003–3010. [CrossRef]

40. Chen, H.; Liang, H.; Dai, W.; Lu, C.; Ding, K.; Bi, J.; Zhu, B. MgScH15: A highly stable cluster for hydrogen storage. *Int. J. Hydrogen Energy* **2020**, *45*, 32260–32268. [CrossRef]
41. Becke, A.D. Density-functional thermochemistry. III. The role of exact exchange. *J. Chem. Phys.* **1993**, *98*, 5648–5652. [CrossRef]
42. Perdew, J.P.; Burke, K.; Wang, Y. Generalized gradient approximation for the exchange-correlation hole of a many-electron system. *Phys. Rev. B.* **1996**, *54*, 16533–16539. [CrossRef] [PubMed]
43. McLean, A.D.; Chandler, G.S. Contracted Gaussian-basis sets for molecular calculations. 1. 2nd row atoms, Z = 11–18. *J. Chem. Phys.* **1980**, *72*, 5639–5648. [CrossRef]
44. Raghavachari, K.; Trucks, G.W. Highly correlated systems: Excitation energies of first row transition metals Sc-Cu. *J. Chem. Phys.* **1989**, *91*, 1062–1065. [CrossRef]
45. Frisch, M.J.; Trucks, G.W.; Schlegel, H.B.; Scuseria, G.E.; Robb, M.A.; Cheeseman, J.R.; Scalmani, G.; Barone, V.; Petersson, G.A.; Nakatsuji, H.; et al. *Gaussian 16, Revision C.01*; Gaussian, Inc.: Wallingford, CT, USA, 2016.
46. Glendening, E.D.; Badenhoop, J.K.; Reed, A.E.; Carpenter, J.E.; Bohmann, J.A.; Morales, C.M.; Karafiloglou, P.; Landis, C.R.; Weinhold, F. *NBO, 7.0*; Theoretical Chemistry Institute, University of Wisconsin: Madison, WI, USA, 2018.
47. Dennington, R.; Keith, T.A.; Millam, J.M. *GaussView, Version 6.0.16*; Semichem Inc.: Shawnee Mission, KS, USA, 2016.